Biosensors and Bioelectronics 144 (2019) 111637

Contents lists available at ScienceDirect

Biosensors and Bioelectronics

journal homepage: www.elsevier.com/locate/bios

Wearable biomolecule smartsensors based on one-step fabricated berlin green printed arrays

Junlin Ma, Yu Jiang, Liuxue Shen, Hongting Ma, Tongrui Sun, Fengjuan Lv, Almas Kiran, Nan Zhu*

Zhang Dayu School of Chemistry, Dalian University of Technology, Dalian, Liaoning, 116024, China

ARTICLE INFO

Keywords:
Berlin green
Hydrogen peroxide sensor
Glucose sensor
Wearable biomolecule sensor
Smartsensor

ABSTRACT

The wearable smart detection of body biomolecules and biomarkers is being of significance in the practical fields. Hydrogen peroxide (H_2O_2) is a product of some enzyme-catalyzed biomolecular reactions. The detection of H_2O_2 could reflect the concentration information of the enzyme reaction biomolecule substrate such as glucose. A high-performance berlin green (BG) carbon ink for monitoring H_2O_2 was prepared in this work. And we have successfully developed the wearable smartsensors for detecting H_2O_2 and glucose based on one-step fabricated BG arrays by screen-printing technology. Comparing with other detection methods, these sensors are wearable, movable, flexible and biocompatible for monitoring biomolecules. As a result, the sensors exhibited good sensitivity, specificity, stability and reproductivity towards H_2O_2 and glucose. Additionally, there also received stable response after near one hundred times stretching and thousands of bending. Moreover, the wearable sensors could be easily remotely controlled by a smart phone, when integrated with wireless into the device. In prospective studies, the one-step fabricated wearable smartsensors is of great significance in developing a straightforward, highly-efficient and low-cost method for actual detection of biomolecules reflecting body health status, and would potentially be applied in the artificial intelligence (AI) fields.

1. Introduction

In the past decades, wearable sensing devices have developed rapidly in the fields of health (Gao et al., 2016; Honda et al., 2014; Wang et al., 2013), medical care (Patel et al., 2012; Tai et al., 2018) and motion (Dobkin and Dorsch, 2011; Jung et al., 2014). With the Internet of Things (IoT) and Artificial Intelligence (AI) emerging, there presents exciting opportunities for wearable sensors to apply into numerous aspects of human daily life. Some researchers have combined biosensors with intelligent products into practice. For instance, a simple enzyme-based alcohol sensor has been fabricated through a Bluetooth transmitter, receiving signals with a smartphone (Kim et al., 2016).

These enzyme-based biosensors can be used for detecting the corresponding substrates such as biomarkers including uric acid (Liao et al., 2015), glucose (Bandodkar et al., 2015a), lactic acid (Kim et al., 2014) and cholesterol (Ruecha et al., 2014), etc. The concentration indexes could normally response the information of human health. For example, the glucose detection in sweat or interstitial fluid can reflect blood glucose levels, which has obtained great attention in diabetes management (Kim et al., 2018; Lee et al., 2017). The biosensors provided continuous, non-invasive and real-time monitoring, with excellent selectivity and identification to prevent the interference of irrelevant substances (Garcia-Carmona et al., 2017). Generally, most biosensors obtain the concentration information of substrates depending on the quantification of hydrogen peroxide (H_2O_2), a kind of side products resulting from most enzyme-catalyzed reactions. (Ricci and Palleschi, 2005; Wilson and Hu, 2000; Zhu et al., 2013)." Furthermore, H_2O_2 is also of significance in clinical application, pharmaceutical, environmental areas, food manufacturing and diagnosis of diseases (Chen et al., 2014; Li et al., 2016b; Zhang et al., 2009). Hence, there plays an essential role in monitoring H_2O_2 both in enzyme-based biosensors or devices and practical fields. In this regard, electrochemical sensing of H_2O_2 is a simple, prompt, sensitive, and cost-effective technology, comparing with conventional methods as fluorescence spectroscopy (Gomes et al., 2005), spectrophotometry (Nogueira et al., 2005), chem-iluminescence (Hanaoka et al., 2001), *etc*.

A series of materials (e.g., redox proteins (Zhao et al., 2005), polymers (Li et al., 2016a), transition metals (Guo et al., 2009), metal oxides (Wei and Wang, 2008), etc.) have been employed to detect H_2O_2 by electrochemical sensors. Ideally, electroactive materials ought to

* Corresponding author.
E-mail address: nanzhu@dlut.edu.cn (N. Zhu).

https://doi.org/10.1016/j.bios.2019.111637
Received 25 June 2019; Received in revised form 25 August 2019; Accepted 26 August 2019
Available online 29 August 2019
0956-5663/

perform a good catalytic activity at a relatively low potential. Prussian blue (PB) has been extensively pursued exciting electrocatalytic sensing behaviour of H_2O_2 (Karyakin et al., 2000; Komkova et al., 2018; Nossol and Zarbin, 2009) since Neff first reported its electrochemical properties in 1978 (Neff, 1978). Similarly, as a typical nanocrystal of PB structure, berlin green (BG) with a formula of $FeFe(CN)_6$ (Shadike et al., 2017) has been widely applied in energy storage (Wu et al., 2015; You et al., 2014), as well as has potential significance in H_2O_2 electrocatalytic sensing. PB nanocrystals perform amperometric detection of H_2O_2 at the low potential of around −50 mV (vs Ag/AgCl), effectively avoiding interference of biological molecules such as uric acid and ascorbic acid (Ricci and Palleschi, 2005; Karyakin, 2015). However, PB nanocrystals are normally modified on the electrodes by traditional electrochemical processes such as drop coating (Bonacin et al., 2017), electrodeposition (Lu et al., 2017), and inkjet printing (Cinti et al., 2015), which are time-consuming, complicated or poor repeatable. Regarding one-step prepared electrodes without further modification, screen printing technology provides a promising pathway to develop an efficient, low cost and easily manufactured sensing method. On the other hand, as an important part of printed electronics, screen printed electrochemical devices could also be combined with a flexible integrated electronic or wireless in various utility fields (Bandodkar et al. 2013, 2015b, 2016; Carrilho et al., 2009).

In the present study, we have synthesized highly electrocatalytic berlin green nanoparticles (BGNPs) and one-step prepared BG carbon ink (BGC ink) by grinding assemble. Based on the BGC ink, wearable H_2O_2 sensor and glucose sensor have been fabricated, utilizing polyethylene glycol terephthalate (PET) and nitrile glove platforms via screen printing technology. Moreover, electrocatalytic behaviors of sensitivity, stability and reproductivity have been expressed in this work. As wearable devices, the stretching and bending performance have also been discussed here. What is more interesting, the wearable sensors could easily be remotely controlled by a smartphone for real-time detection of the corresponding analytes, when integrated with wireless into the device. In a word, we have developed BGC-based wearable smart H_2O_2 and glucose sensors, which is promising in detecting body biomolecules and potentially applied in the intelligent fields.

2. Experimental section

2.1. Materials and reagents

Carbon ink ch-8 (mod2, Jujo printing supplies & technology), commercially available polyethylene glycol terephthalate (PET), conductive silver adhesive, wire, blue nitrile powder-free exam gloves (Ammex) were used as received. Ag/AgCl ink was purchased from Shanghai Baoyin Co., Ltd (BY–2000H, Shanghai, China), insulating ink was supplied by shanghai Jin-Yi Screen Printing Equipment Co., Ltd (Shanghai, China). Potassium hexacyanoferrate (III) ($K_3[Fe(CN)_6]$, ≥99%), ferric chloride ($FeCl_3$ ≥99%), hydrochloric acid (HCl), acetic acid, potassium chloride (KCl ≥99%), sodium phosphate monobasic dehydrate (NaH_2PO4, ≥99%) and disodium hydrogen phosphate dodecahydrate (Na_2HPO4, ≥99%) were obtained from Damao chemical reagent factory (Tianjin, China). Hydrogen peroxide (H_2O_2, 30%) from Tjkermel (Tianjin, China) was used. Chitosan (CAS: 9012-76-4), bovine serum albumin (BSA, CAS: 9048-46-8), D-(+)-glucose (≥99.5%), and glucose oxidase of Aspergillus niger (expressed as GOD or GOx, CAS: 9001-37-0) were purchased from Aladdin (Shanghai, China).

2.2. Synthesis of BGNPs

The BGNPs were prepared by using $[Fe(CN)_6]^{3-}$ and Fe^{3+} as iron-source. In brief, 50 mM $FeCl_3$ solution (20 mL) containing 0.1 M KCl was mixed with concentrated HCl (1 mL). Subsequently, 50 mM $K_3[Fe(CN)_6]$ (20 mL) was dropwisely added into the mixed solution under vigorous stirring at room temperature for 40 h. Then BGNPs were collected by centrifugation, and further washed by deionized water and alcohol for several times. Finally, BGNPs were dried overnight.

2.3. Preparation of the BGC ink

Typically, 20 mg BGNPs was dispersed into 120 μL deionized water in a mortar. Thereafter, 3 g carbon ink was added into the mixture by adequately grinding. It should be pointed out that the amount of each material could be freely adjusted when the proportion was fixed.

2.4. Fabrication of PET-based H_2O_2 sensor

The electrodes of sensor were fabricated using a commercial manual screen printer. These sensor patterns include working electrode (WE), reference electrode (RE) and counter electrode (CE), were designed in the AutoCAD software and processed into stainless steel stencils. Here, pure carbon ink or BGC ink was used to prepare WE and CE, Ag/AgCl ink was used to prepare RE. The attached impurity of PET substrate should be removed with acetone in an ultrasonic bath for 30 min. Subsequently, Ag/AgCl ink and BGC ink were printed in sequence to complete electrochemical sensors. In this process, layers of Ag/AgCl ink were cured at 80 °C for 30 min and BGC ink were cured at 120 °C for 5 min. Afterwards, manufacturing insulating layer by printing insulating ink as an insulation to confining the exact size of electrode array, and cured at 120 °C for 2 h. Finally, the sensor array was stuck to the wire with the help of conductive silver for further electrochemical detecting.

2.5. Fabrication of PET-based glucose sensor

The glucose sensor was fabricated by functionalizing PET-based working electrode with GOD. The GOD solution was prepared as follows. Firstly, 35 mg GOD was dispersed in 1 mL PBS containing 10 mg BSA stabilizer. Secondly, 1 wt % of chitosan and 2 v% of acetic acid were dissolve in PBS. Finally, they were mixed in a 1:1 v/v ratio. Subsequently, a 4 μL droplet of this solution was casted on the working electrode and dried under ambient conditions. Afterwards, glucose sensor was stored at 4 °C.

2.6. Fabrication of wearable glove-based H_2O_2 and glucose sensors

The fabrication process of glove-based H_2O_2 sensors was similar to PET-based sensor. Firstly, PET was replaced by nitrile glove. Secondly, screen printing of the sensor arrays. Thirdly, the insulating ink was used for integrating insulating layer. At the same time, the 3D printed finger molds were put into the glove to ensure smoothness of glove surface. The fabrication process of glove-based glucose sensors was the same as PET-based sensors.

2.7. Characterization analysis

The powder X-ray diffraction (XRD) measurements were on a Rigaku D/MAX-2400 diffractometer. UV–vis measurements were carried out using a Cary Series UV–vis Spectrophotometer. Scanning electron microscope images (SEM) and elemental mappings were measured on a Nova Nanosem 450 field emission scanning electron microscope (FE-SEM) at 3 kV to investigate the morphology of working electrode surface. Transmission electron microscopy(TEM) was performed using a Philips Tecnai G2F20.

2.8. Electrochemical measurements and mechanical performance studies

All electrochemical measurements were carried out at room temperature by using CHI 660D electrochemical workstation. All of electrochemical measurements used 0.05 M PBS (pH7.4) containing 0.1 M

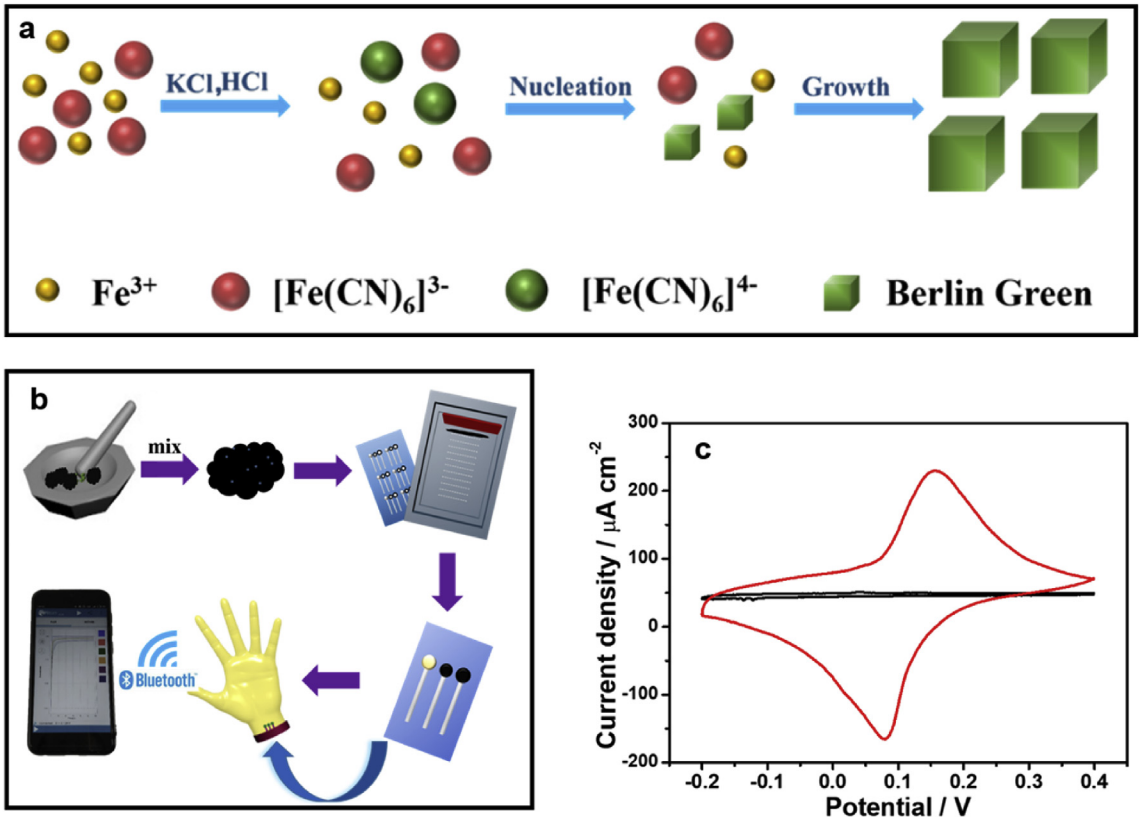

Fig. 1. Preparation of BGNPs and experimental procedure. (a) Nucleation diagram of preparing BGNPs. (b) Schematic illustration of the detailed experimental process. (c) Comparison of CVs of carbon ink (black curve) and BGC ink (red curve), scan rate 50 mV s − 1. Electrolyte: 0.05 M phosphate buffer (pH 7.4) containing 0.1 M KCl used in all the electrochemical measurements. (For interpretation of the references to color in this figure legend, the reader is referred to the Web version of this article.)

KCl. In addition, Emstat blue, a PalmSens connected with a smart phone via Bluetooth, was used to collect wireless data. Employing amperometric curves measurements to study the effect of stretching and bending performance on the printed nitrile gloves.

3. Results and discussion

3.1. Fabrication and characterization of BGNPs and BGC ink

The synthesis process of BGNPs, BGC ink preparation and the specific wireless wearable sensor manufacturing procedure were illustrated Fig. 1a and b. Firstly, the synthesis of BGNPs mimics electrodeposition (Ellis et al., 1981) and follows a slow reaction between $FeCl_3$ and $K_3[Fe(CN)_6]$ at room temperature (Fig. 1a and Experimental Section). In the presence of HCl, $FeFe(CN)_6$ nanocrystals (BGNPs) were precipitated by undecomposed $Fe(CN)_6^{3-}$ associate with Fe^{3+} derived from $Fe(CN)_6^{3-}$ and $FeCl_3$ (Wu et al., 2016). The as-prepared BGNPs were composed of cubic nanoparticles with a uniform size of about 150 nm from SEM and TEM images (Fig. 2a and b). Moreover, the BGNPs were well dispersed in deionized water, which exhibited green color with three absorption peaks of around 300, 420 and 760 nm by UV–Vis spectroscopy (Figs. S1a and b). The absorption peak of 300 and 420 nm are ligand-to-metal charge transfer in the ferricyanide ion (Braterma.Ps, 1966; Robin, 1961). In addition, the absorption at 700 nm persisted due to the fact that part of the ferrocyanide ion remained unoxidized (Itaya et al., 1982; Wu et al., 2016). The X-ray diffraction (XRD) peaks of BGNPs were indexed to a face-centered cubic lattice with a space group of $Fm\bar{3}m$ (JCPDS no. 73–0687, Fig. 2c) (Shadike et al., 2017; Wu et al., 2015), reflecting the structural regularity of BG from the strong and sharp diffraction peaks.

Subsequently, BGC inks were obtained by above BGNPs and carbon ink sufficiently grinding, so that BGNPs were uniformly dispersed into carbon materials. Significantlly, it is critical to control the ratio of each component. If BGNPs is excessive, the conductivity of the ink would be so poor that slower the electron transfer of electrocatalysis; on the contrary, poor electrocatalytic performance would be exhibited (The optimal experiments were given in Table S1, Fig. S2 and Fig. S3). Although there contained extremely low percentage of BGNPs in the mixture, BGC ink still showed slight diffraction peaks of BGNPs from XRD (Fig. 2d and Fig. S4). The BGC showed the planes of (200), (400) and (420) in the magnified image of Fig. 2d, corresponding to 2θ of 17.5, 35.4 and 39.8°, respectively. Comparing to pure carbon ink, there also appeared clearly BGNPs in the BGC ink from SEM image (Fig. 2e and f), indicating that BGNPs were finely incorporated into carbon ink. Elemental mappings were further carried out to prove the results. Pure carbon ink only contained the elements of C and O (Fig. S5a), while both BGNPs and BGC ink contained the elements of C, O and Fe (Figs. S5b and c). However, the element of N was not observed in BGC ink, presumably due to the relatively low amount of BGNPs in the mixture. The elemental mappings as well confirmed the successful preparation of BGC ink as expected.

3.2. Electrochemical behaviors of H_2O_2 and glucose sensors

As discussed in the introduction, BG is a kind of PB nanocrystals, so BGC ink would exhibit considerable electrochemical performance as PB. The crown patterned BGC electrodes have been fabricated on PET substrate by screen printing. The electrochemical and sensing properties of the sensors were measured utilizing cyclic voltammetry (CV) and amperometic i-t curves. As a result, a notable pair of typical redox peaks was observed at around 0.16 V and 0.08 V during the electrochemical process in the CV (Fig. 1c), representing the PB/PBred (prussian white,

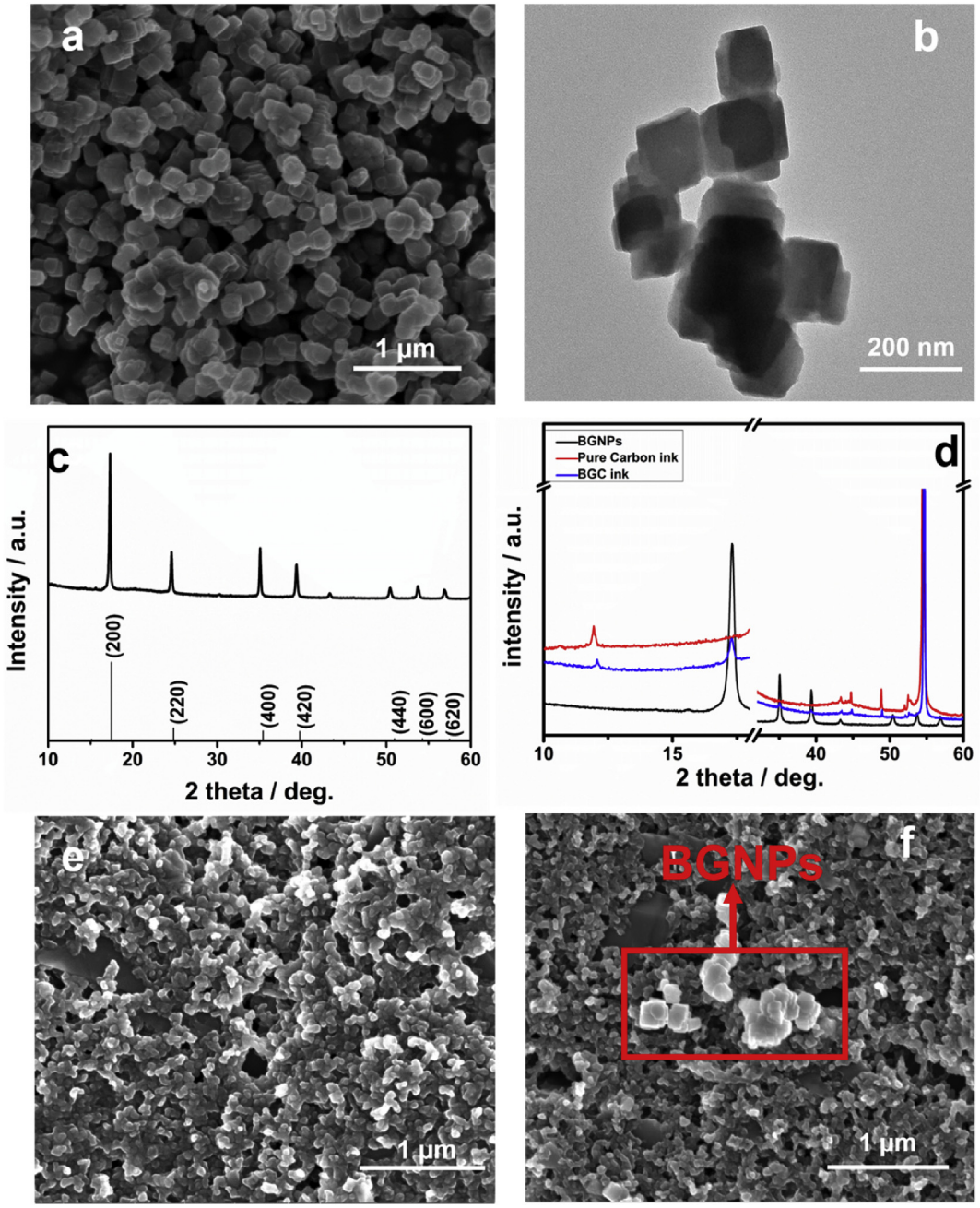

Fig. 2. Characterization of BGNPs and BGC ink. (a) SEM image and (b) TEM image of the BGNPs; (c) The XRD pattern of BGNPs; (d) The XRD patterns of BGNPs (black curve), BGC ink (blue curve) and pure carbon ink (red curve); (e) SEM image of pure carbon ink; (f) SEM image of BGC ink. (For interpretation of the references to color in this figure legend, the reader is referred to the Web version of this article.)

PW) redox couple (Karyakin, 2015). Thus, BGC ink performed reliable electrochemical behaviors. Meanwhile, the peak current of cathode and anode increased linearly with the scan rates, indicating that the process was diffusionless electrochemical reactions (Figs. S6a and b) (Zhu et al., 2016). Hence, it is expected that this kind of sensor will perform well in homogeneous solution.

In the presence of 10 mM H_2O_2, there exhibited well-defined electrocatalytic reduction of H_2O_2 starting at 0 V (*vs.* Ag/AgCl) by CV, comparing with absence of H_2O_2 (Fig. 3a). With the raising concentration of H_2O_2, the electrocatalytic current will increase proportionally in CVs (Fig. S7a). Furthermore, regarding a low potential for H_2O_2 reduction of this sensor, amperometic curves were evaluated over the concentration range of 1–10 mM H_2O_2 at a fixed potential of −0.05 V (de Mattos et al., 2003; Ricci et al., 2003; Li et al., 2016b) in the measurement (Fig. 3b). Then, this H_2O_2 sensor expressed an excellent linear relationship with a sensitivity of 27.25 μA mM^{-1} cm^{-2} and a detection limit of 0.65 μM (Fig. 3c). There achieved saturated in the higher concentration of 20 mM, similar to an enzyme reaction process (Fig. S7b) (Cinti et al., 2014). The performance of this one-step BGC H_2O_2 sensor was significantly better than the previous study of insoluble PB nanoparticles modified on the electrode surface with a piezoelectric inkjet printer (Hu et al., 2012). Interestingly, this BGC H_2O_2 sensor expressed a good stability for continuous 20 cycles testing at 10 mM H_2O_2, with a low relative standard deviation (RSD) of 5.2% (Fig. 3d). This could be attributed to an excellent combination between BGNPs and carbon ink in a suitable ratio. In addition, there also illustrated a good reproductivity of sensitivity by different screen-printed electrodes with a low RSD of 5.8% (Fig. S8). For practical application,

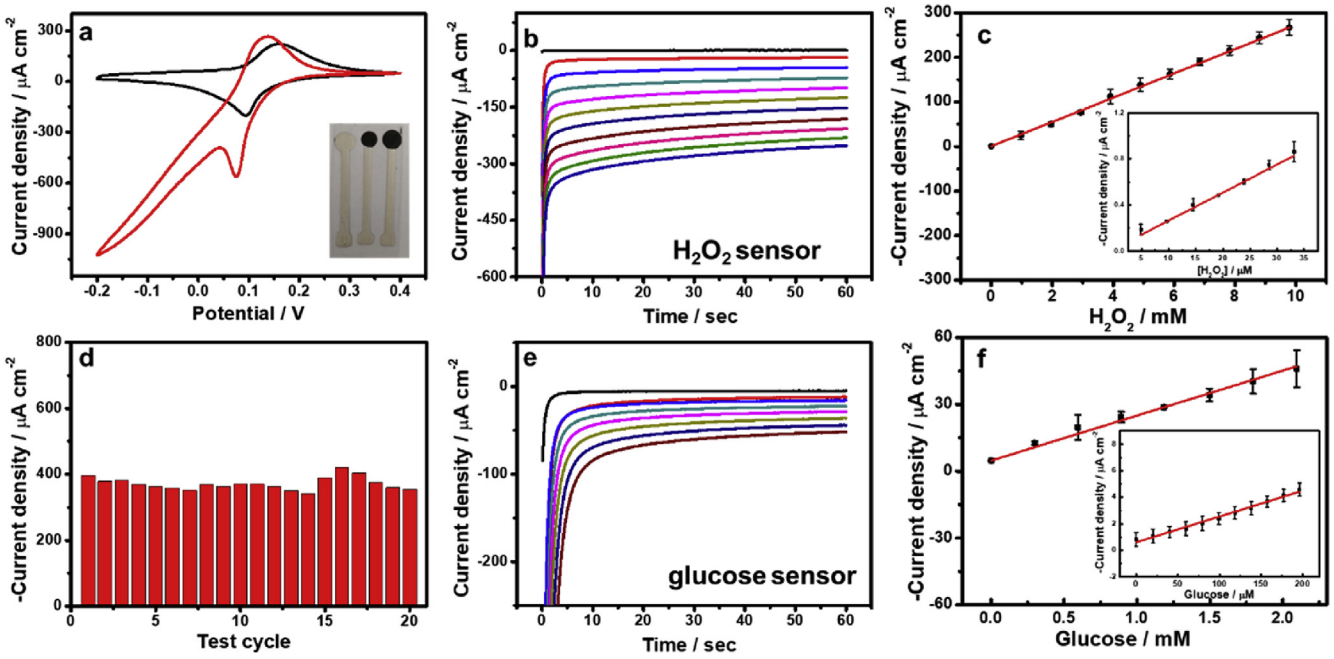

Fig. 3. Electrochemical properties of H2O2 and glucose sensors. (a) CVs of BGC-PET-based sensor in the absence (black curve) and presence (red curve) of 10 mM H2O2 at 50 mV s-1; the inset was the actual electrode diagram. (b) Amperometric i-t curves of the BGC-PET-based sensor responding to H2O2 with the concentration between 0 mM and 10 mM in 1 mM increments. (c) Linear relationship of H2O2 sensor collected at 60s; the inset was in the extremely low concentration. (d) Stability of sensor arrays by recording at 10 mM H2O2 during 20 repetitive runs (RSD = 5.2%). (e) Amperometric i-t curves of the BGC-PET-based glucose sensor with the concentration between 0 mM and 2.1 mM in 0.3 mM increments. (f) Linear relationship of glucose collected at 60s; the inset was recorded at extremely low concentration of glucose. Electrolyte: 0.05 M phosphate buffer (pH 7.4) containing 0.1 M KCl. All i-t curves were carried out at −0.05 V vs. Ag/AgCl. (For interpretation of the references to color in this figure legend, the reader is referred to the Web version of this article.)

some other interfering substances (i.e. ascorbic acid, uric acid, etc.) would be usually simultaneously present in real samples, which might also give interfering signals. So, the specificity of PET-based H_2O_2 sensor has been evaluated. As shown in Fig. S9a, there appeared barely changed of H_2O_2 sensor after adding 1 mM of uric acid (UA), dopamine (DA) and ascorbic acid (AA), respectively. On contrary, the current changed significantly of 1 mM H_2O_2.

Subsequently, BGC-based redox enzyme sensors have been fabricated as a biosensing device. In this work, taking the most popular natural substrate of glucose as an example for discussing the enzyme electrocatalysis by this sensor. The entire BGC-based glucose catalytic process can be expressed by Equations (1) and (2). Firstly, glucose oxidase (GOD) oxidized glucose to form gluconic acid and H_2O_2 in the presence of oxygen. In the second step, generated H_2O_2 was catalyzed by PB_{red}, derived from BG nanocrystal (Bandodkar et al., 2015a). As is well known, the glucose information will be indirectly recorded by measuring H_2O_2 from the above equations.

$$Glucose + O2 \overset{GOx}{\rightarrow} Gluconic\ acid + H2O2 \quad (1)$$

$$PBred + H2O2 \rightarrow PBox + OH- \quad (2)$$

As a result, the glucose sensors exhibited good electrochemical sensing properties by amperometric i-t curves, corresponding to the concentration of glucose from 0 to 2.1 mM (Fig. 3e). And they not only showed an excellent linear relationship between current density and glucose concentration, but also with a sensitivity of 20.22 μA mM^{-1} cm^{-2} and a detection limit of 11.6 μM (Fig. 3f), which were superior to the similar literatures (Moscone et al., 2001; O'Halloran et al., 2001). Surprisingly, this enzyme-based glucose sensor had good specificity, which can avoid the influence of interfering substances in actual detection. It can be found from Fig. S9b that almost no changes were observed after adding 1 mM of AA, UA, DA, D-alanine and NaCl, respectively. However, significant change occurred of 1 mM glucose. In addition, Thanks to the use of chitosan and bovine serum albumin (BSA) during the preparation, resulting into better adhesion of enzyme to the sensor and better catalytic effects with the substrate. Moreover, the results of relationship between current and glucose concentration were in accordance with the Michaelis-Menten equation (Fig. S10), and the apparent Michaelis-Menten constant (K_M) was estimated as 2.67 mM. The value of K_M was lower than reported literatures (Kimmel et al., 2012; Salimi et al., 2007), suggesting that BGC glucose sensor had a high binding affinity to the substrate. Therefore, besides glucose, this BGC sensor would also have the prospect to detect other body biomolecules when modified other oxidases in the practical application.

3.3. Wearable H_2O_2 and glucose smartsensors

The wearable integrated BGC sensors have been fabricated on the nitrile gloves by screen printing. Similarly, this wearable sensor also exhibited typical redox peaks of PB nanocrystals, compared with pure carbon ink (Fig. 4a). As expected, this wearable H_2O_2 sensor displayed excellent sensitivity towards the concentration from 1 to 10 mM until saturated (Fig. 4b), similar to the properties of PET-based sensor. Particularly, due to the diffusion rates of different substrates, the sensitivity of glove-based sensor was slightly lower than PET-based sensors (Jiang et al., 2019). Furthermore, the stretching and bending performance of wearable H_2O_2 sensor have been studied in the practical use. The stretching measurement was carried out by 10% stretching, remaining a relatively stable response after 70 cycles (Fig. 4c). And after 1800 consecutive 90° bending cycles, this wearable sensor still demonstrated good stability (Fig. 4d). The actual operated photos during stretching and bending process were displayed in the inset of Fig. 4c and d, respectively.

Thereafter, the wearable glucose sensor has been developed in realizing highly flexible biosensor device. It also displayed a linear dependence between current and glucose concentration by amperometric detection (Fig. S11a), being consistent with the PET-based

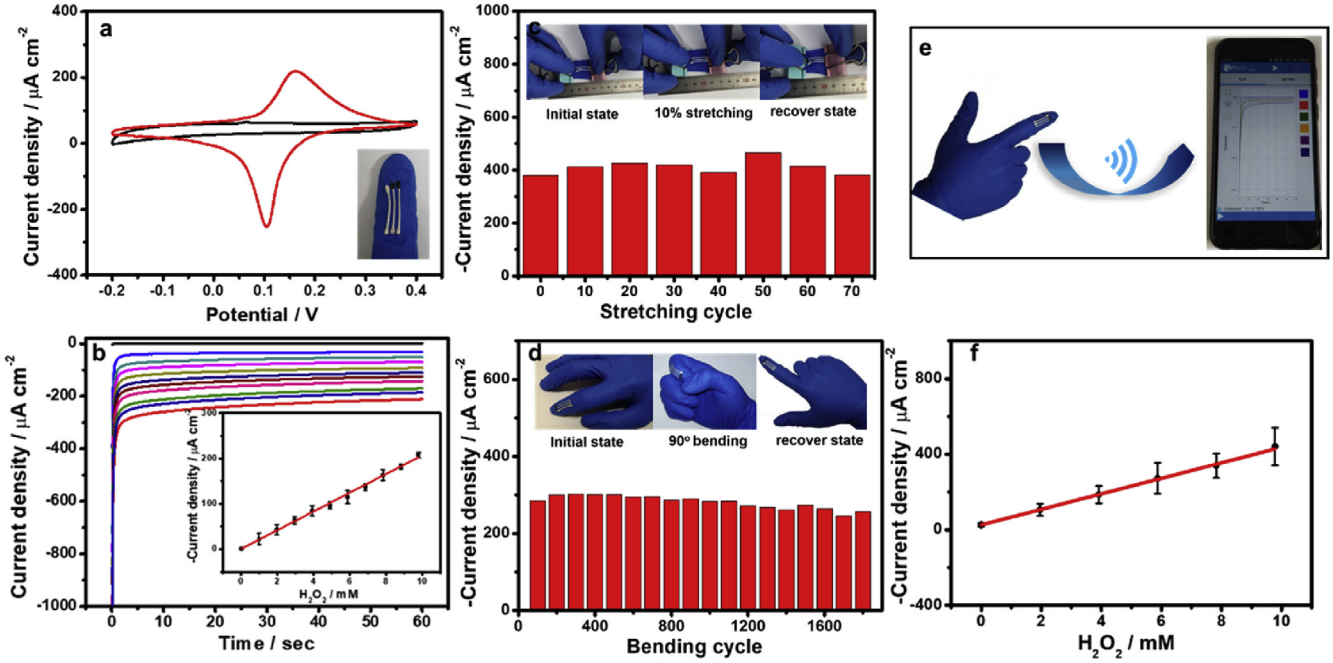

Fig. 4. The behaviors of wearable biomolecule smartsensors. (a) Comparison of CVs between BGC ink (red curve) and carbon ink (black curve) by the glove sensor, scan rate 50 mV s − 1; the inset was the actual electrode diagram. (b) Amperometric i-t curves of wearable H2O2 sensor with the concentration between 0 mM and 10 mM in 1 mM increments; the inset was linear relationship of H2O2 collected at 60s. (c) Stretching test of 10% stretch recorded every 10 cycles (RSD = 6.86%). (d) Bending test of 90° bending recorded every 100 cycles (RSD = 6.37%). (e) Schematic diagram of wearable smartsensor measured by a mobile phone. (f) Linear relationship of H2O2 in the range 0–10 mM from mobile APP. Electrolyte: 0.05 M phosphate buffer (pH 7.4) containing 0.1 M KCl. All of i-t curves were carried out at − 0.05 V vs. Ag/AgCl. (For interpretation of the references to color in this figure legend, the reader is referred to the Web version of this article.)

glucose sensor. Meanwhile, the apparent Michaelis-Menten constant from the Michaelis-Menten equation was estimated as 2.65 mM (Fig. S11b), indicating a highly binding affinity to glucose by this wearable glucose sensor. Based on H_2O_2 and glucose detection, the wearable sensor would have a potential application for other biological samples.

When the wearable sensor was integrated with wireless, electrochemical signals would also be easily obtained by a smart phone to remotely control. Wearable smart H_2O_2 sensor and glucose sensor have been both acquired (Fig. 4e), and there displayed reliable sensitivity and good linear relationship either H_2O_2 (Fig. 4f) or glucose (Fig. S12). In other words, the wearable smartsensors have provided a convenient and simple technology for monitoring body biomolecules such as glucose by a remotely precise detection.

4. Conclusions

In conclusion, we have successfully fabricated wearable H_2O_2 and glucose smartsensors based on one-step prepared BGC printed inks. There received a simple, efficient and low-cost integrated sensor by screen printing technology. Thanks to the successful preparation of BGC inks, BGC-based H_2O_2 sensors and glucose sensors exhibited good stability and reproductivity, as well as excellent sensitivity of with $27.25\,\mu A\,mM^{-1}\,cm^{-2}$ and $20.22\,\mu A\,mM^{-1}\,cm^{-2}$, respectively. Moreover, without pre-treatment or adding any polymers into inks, the wearable glove-based sensors remained a relatively stable response after 70 cycles by 10% stretching and after 1800 consecutive 90° bending cycles. When the wearable sensors were integrated with wireless devices, we could also remotely acquire similar results through a smartphone for detecting H_2O_2 and glucose. Therefore, this one-step prepared wearable sensor would provide a simple and convenient method to develop active materials combining into the inks, and offer the opportunity to fabricate wearable wireless sensors for monitoring H_2O_2 and glucose. In prospective studies, the present work has the promise to develop straightforward, highly-efficient and low-cost fabrication of wearable smartsensors for actual detection of biomolecules.

CRediT authorship contribution statement

Junlin Ma: Formal analysis, Writing - original draft. **Yu Jiang:** Formal analysis. **Liuxue Shen:** Formal analysis. **Hongting Ma:** Formal analysis. **Tongrui Sun:** Formal analysis. **Fengjuan Lv:** Formal analysis. **Almas Kiran:** Formal analysis. **Nan Zhu:** Conceptualization, Methodology, Resources, Project administration, Writing - original draft, Writing - review & editing, Supervision, Funding acquisition.

Declaration of competing interest

The authors declare that they have no known competing financial interests or personal relationships that could have appeared to influence the work reported in this paper.

Acknowledgements

We are grateful for the financial support from National Natural Science Foundation of China [Grant No. 21705014], the Fundamental Research Funds for Central Universities [Grant No. DUT18LK56], Natural Science Foundation of Liaoning Province, China [Grant No. 20180510060], Dalian Science and Technology Innovation Project, China [Grant No. 2019J12SN54], and Zhang Dayu School of Chemistry, Dalian University of Technology, China.

Appendix A. Supplementary data

Supplementary data to this article can be found online at https://doi.org/10.1016/j.bios.2019.111637.

References

Braterma, Ps, 1966. J. Chem. Soc. A (10), 1471.
Bandodkar, A.J., O'Mahony, A.M., Ramirez, J., Samek, I.A., Anderson, S.M., Windmiller, J.R., Wang, J., 2013. Analyst 138 (18), 5288–5295.

Bandodkar, A.J., Jia, W., Yardimci, C., Wang, X., Ramirez, J., Wang, J., 2015a. Anal. Chem. 87 (1), 394–398.
Bandodkar, A.J., Nunez-Flores, R., Jia, W., Wang, J., 2015b. Adv. Mater. 27 (19), 3060–3065.
Bandodkar, A.J., Jeerapan, I., You, J.M., Nunez-Flores, R., Wang, J., 2016. Nano Lett. 16 (1), 721–727.
Bonacin, J.A., Dos Santos, P.L., Katic, V., Foster, C.W., Banks, C.E., 2017. Electroanalysis 30 (1).
Carrilho, E., Martinez, A.W., Whitesides, G.M., 2009. Anal. Chem. 81 (16), 7091–7095.
Chen, S., Hai, X., Chen, X.W., Wang, J.H., 2014. Anal. Chem. 86 (13), 6689–6694.
Cinti, S., Arduini, F., Moscone, D., Palleschi, G., Killard, A.J., 2014. Sensors 14 (8), 14222–14234.
Cinti, S., Arduini, F., Moscone, D., Palleschi, G., Gonzalez-Macia, L., Killard, A.J., 2015. Sens. Actuators, B 221, 187–190.
de Mattos, I.L., Gorton, L., Ruzgas, T., 2003. Biosens. Bioelectron. 18 (2–3), 193–200.
Dobkin, B.H., Dorsch, A., 2011. Neurorehabilitation Neural Repair 25 (9), 788–798.
Ellis, D., Eckhoff, M., Neff, V.D., 1981. J. Phys. Chem. 85 (9), 1225–1231.
Gomes, A., Fernandes, E., Lima, J.L., 2005. J. Biochem. Biophys. Methods 65 (2–3), 45–80.
Guo, S., Wen, D., Dong, S., Wang, E., 2009. Talanta 77 (4), 1510–1517.
Gao, W., Emaminejad, S., Nyein, H.Y.Y., Challa, S., Chen, K., Peck, A., Fahad, H.M., Ota, H., Shiraki, H., Kiriya, D., Lien, D.H., Brooks, G.A., Davis, R.W., Javey, A., 2016. Nature 529 (7587), 509–514.
Garcia-Carmona, L., Moreno-Guzman, M., Gonzalez, M.C., Escarpa, A., 2017. Biosens. Bioelectron. 96, 275–280.
Hanaoka, S., Lin, J.-M., Yamada, M., 2001. Anal. Chim. Acta 426 (1), 57–64.
Hu, J.-Y., Lin, Y.-P., Liao, Y.-C., 2012. Anal. Sci. 28 (2), 135.
Honda, W., Harada, S., Arie, T., Akita, S., Takei, K., 2014. Adv. Funct. Mater. 24 (22), 3299–3304.
Itaya, K., Ataka, T., Toshima, S., 1982. J. Am. Chem. Soc. 104 (18), 4767–4772.
Jung, S., Lee, J., Hyeon, T., Lee, M., Kim, D.H., 2014. Adv. Mater. 26 (36), 6329–6334.
Jiang, Y., Ma, J., Lv, J., Ma, H., Xia, H., Wang, J., Yang, C., Xue, M., Li, G., Zhu, N., 2019. ACS Sens. 4 (1), 152–160.
Karyakin, A.A., Karyakina, E.E., Gorton, L., 2000. Anal. Chem. 72 (7), 1720–1723.
Kimmel, D.W., LeBlanc, G., Meschievitz, M.E., Cliffel, D.E., 2012. Anal. Chem. 84 (2), 685–707.
Kim, J., Valdes-Ramirez, G., Bandodkar, A.J., Jia, W., Martinez, A.G., Ramirez, J., Mercier, P., Wang, J., 2014. Analyst 139 (7), 1632–1636.
Karyakin, A.A., 2015. Electroanalysis 13 (10), 813–819.
Kim, J., Jeerapan, I., Imani, S., Cho, T.N., Bandodkar, A., Cinti, S., Mercier, P.P., Wang, J., 2016. ACS Sens. 1 (8), 1011–1019.
Kim, J., Sempionatto, J.R., Imani, S., Hartel, M.C., Barfidokht, A., Tang, G.D., Campbell, A.S., Mercier, P.P., Wang, J., 2018. Adv. Sci. 5 (10).
Komkova, M.A., Karyakina, E.E., Karyakin, A.A., 2018. J. Am. Chem. Soc. 140 (36), 11302–11307.
Liao, C., Mak, C., Zhang, M., Chan, H.L., Yan, F., 2015. Adv. Mater. 27 (4), 676–681.
Li, P., Kang, H., Zhang, C., Li, W., Huang, Y., Liu, R., 2016a. Carbohydr. Polym. 140, 35–42.
Li, R., Liu, X., Qiu, W., Zhang, M., 2016b. Anal. Chem. 88 (15), 7769–7776.
Lee, H., Song, C., Hong, Y.S., Kim, M.S., Cho, H.R., Kang, T., Shin, K., Choi, S.H., Hyeon, T., Kim, D.H., 2017. Sci. Adv. 3 (3), 1601314.
Lu, S.-Y., Chen, Y., Fang, X., Feng, X., 2017. J. Appl. Electrochem. 47 (11), 1261–1271.
Moscone, D., D'Ottavi, D., Compagnone, D., Palleschi, G., Amine, A., 2001. Anal. Chem. 73 (11), 2529–2535.
Neff, V.D., 1978. J. Electrochem. Soc. 125 (6), 886.
Nogueira, R.F., Oliveira, M.C., Paterlini, W.C., 2005. Talanta 66 (1), 86–91.
Nossol, E., Zarbin, A.J.G., 2009. Adv. Funct. Mater. 19 (24), 3980–3986.
O'Halloran, M.P., Pravda, M., Guilbault, G.G., 2001. Talanta 55 (3), 605–611.
Patel, S., Park, H., Bonato, P., Chan, L., Rodgers, M., 2012. J. NeuroEng. Rehabil. 9, 21.
Robin, M.B., 1961. Spectrochim. Acta 17 (9–10) 1095-1095.
Ricci, F., Amine, A., Palleschi, G., Moscone, D., 2003. Biosens. Bioelectron. 18 (2–3), 165–174.
Ricci, F., Palleschi, G., 2005. Biosens. Bioelectron. 21 (3), 389–407.
Ruecha, N., Rangkupan, R., Rodthongkum, N., Chailapakul, O., 2014. Biosens. Bioelectron. 52, 13–19.
Salimi, A., Sharifi, E., Noorbakhsh, A., Soltanian, S., 2007. Biosens. Bioelectron. 22 (12), 3146–3153.
Shadike, Z., Shi, D.-R., Tian-Wang, T.-W., Cao, M.-H., Yang, S.-F., Chen, J., Fu, Z.-W., 2017. J. Mater. Chem. 5 (14), 6393–6398.
Tai, L.C., Gao, W., Chao, M., Bariya, M., Ngo, Q.P., Shahpar, Z., Nyein, H.Y.Y., Park, H., Sun, J., Jung, Y., Wu, E., Fahad, H.M., Lien, D.H., Ota, H., Cho, G., Javey, A., 2018. Adv. Mater. 30 (23), 1707442.
Wilson, G.S., Hu, Y., 2000. Chem. Rev. 100 (7), 2693–2704.
Wei, H., Wang, E., 2008. Anal. Chem. 80 (6), 2250–2254.
Wang, C., Hwang, D., Yu, Z., Takei, K., Park, J., Chen, T., Ma, B., Javey, A., 2013. Nat. Mater. 12 (10), 899–904.
Wu, X., Luo, Y., Sun, M., Qian, J., Cao, Y., Ai, X., Yang, H., 2015. Nano Energy 13, 117–123.
Wu, X., Shao, M., Wu, C., Qian, J., Cao, Y., Ai, X., Yang, H., 2016. ACS Appl. Mater. Interfaces 8 (36), 23706–23712.
You, Y., Wu, X.-L., Yin, Y.-X., Guo, Y.-G., 2014. Energy Environ. Sci. 7 (5), 1643–1647.
Zhao, Y.D., Bi, Y.H., Zhang, W.D., Luo, Q.M., 2005. Talanta 65 (2), 489–494.
Zhang, L., Li, H., Ni, Y., Li, J., Liao, K., Zhao, G., 2009. Electrochem. Commun. 11 (4), 812–815.
Zhu, N., Han, S., Gan, S., Ulstrup, J., Chi, Q., 2013. Adv. Funct. Mater. 23 (42), 5297–5306.
Zhu, N., Hao, X., Ulstrup, J., Chi, Q., 2016. ACS Catal. 6 (4), 2728–2738.